Meas. Sci. Technol. **8** (1997) 1553–1561. Printed in the UK PII: S0957-0233(97)83910-0

Lagrangian statistics and transilient matrix measurements by PTV in a convective boundary layer

A Cenedese†‡ and G Querzoli§

† DITS, La Sapienza University, Via Eudossiana 18, 00184, Rome, Italy
§ Civil Engineering Department, Tor Vergata University, Via di Tor Vergata, 00133, Rome, Italy

Received 6 May 1997, accepted for publication 30 September 1997

Abstract. The most common velocity measurement techniques, based on image analysis, calculate the velocity by cross-correlation of a portion of the digitized images, and give a Eulerian description of the investigated field. Particle tracking velocimetry (PTV), based on the recognition of trajectories of seeding particles, only furnishes a Eulerian description provided the trajectories are shorter than the characteristic scale of the phenomenon. If particles are tracked for a longer time, a Lagrangian description is obtained. Consequently, in order to successfully evaluate Lagrangian statistics, a long series of single-exposed images has to be acquired. PTV has been used to examine the pollutant dispersion in a laboratory simulation of the convective boundary layer of the atmosphere. The convective layer has been simulated by a water tank heated from below, where the atmospheric thermal stratification has been reproduced. Though the phenomenon was observed to be steady in the Eulerian reference frame, the same did not occur in the Lagrangian reference frame. From the analysis of particle motion, it is possible to determine the characteristic time scale of the turbulence and to describe the different behaviour of hot updraughts and cold downdraughts. The pollutant dispersion is described in detail by the transilient matrix representing the probability of transition of a particle from one level to another of the convective layer. From the information given by this matrix, it is possible, in principle, to estimate the concentration fields, due to a variety of concentrated and distributed pollutant sources.

1. Introduction

Velocity measurement techniques based on image analysis strongly depend on the level of seeding of the working fluid. This level can be defined by first comparing the mean particle distance with the particle displacement between two successive acquisitions and then with the smallest spatial scale of the velocity field structure relevant to the investigation. If the mean distance is much smaller than this scale (high seeding levels), images are analysed by means of the (auto- or cross-) correlation function and this particular technique is called particle image velocimetry (PIV) (Adrian 1991, Keane and Adrian 1992, Lorenço 1996, Raffel and Kompenhans 1996). If the mean distance between particles is of the same order or larger than this scale, statistical analysis over uniform regions is not reliable. In this case, the velocity is obtained from the identification of the trajectory of each particle and this technique is called particle tracking velocimetry (PTV) (Nadeem and Dracos 1993, Querzoli 1996, Virant and Dracos 1996).

‡ E-mail address: gq@cenedese1.ing.uniroma1.it

In PIV, the investigation field is divided into small regions that are individually analysed and one velocity value per region is obtained. This value is representative of the velocity of all the particles found on the analysed area. This means that PIV results in a succession of velocity values at fixed locations, i.e. in a Eulerian description of the velocity field.

Conversely, PTV gives velocity samples along the particle trajectories, that is in a Lagrangian frame of reference. If the length of the trajectories is small compared to the characteristic time scale of the fluid motion, the information is 'locally Lagrangian'. It differs from that obtained from PIV only because the velocity is measured at random locations instead of over a regular grid (one sample per tracked particle is measured rather than averaging over an interrogation area). From the random distribution of samples, the velocity field over a spatial grid can be calculated by interpolation. Nevertheless, there are some phenomena that are naturally described in a Lagrangian frame of reference. For example, in studying pollutant dispersion, the dispersion coefficient can be computed according to Taylor theory from particle displacement statistics (Monin and Yaglom 1971). For the

0957-0233/97/121553+09$19.50

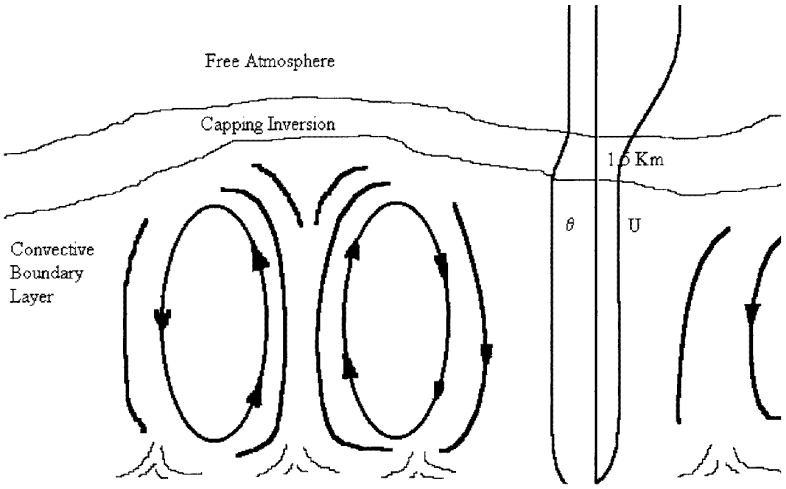

Figure 1. Structure of the atmospheric convective boundary layer. θ is the potential temperature, U the mean wind.

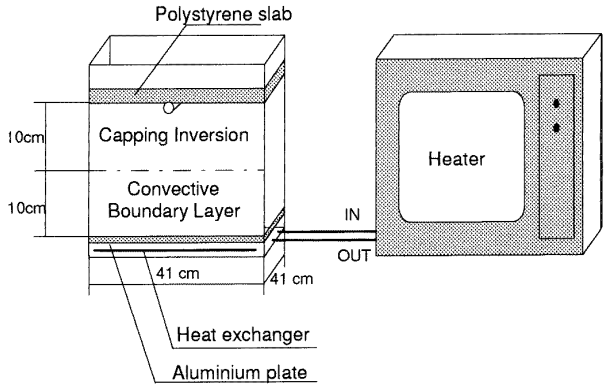

Figure 2. Sketch of the convection chamber and heating system.

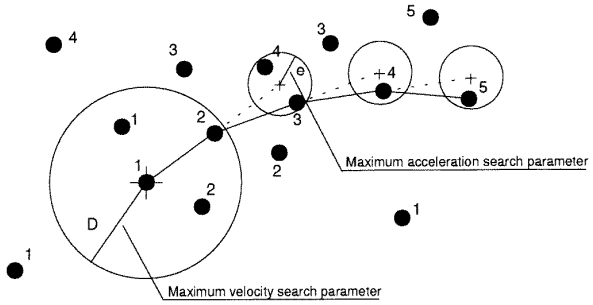

Figure 3. Particle tracking of single-exposed images. Numbers indicate the time of acquisition of the particle centroid locations.

full Lagrangian description, particles have to be tracked for a period of several time scales of the phenomenon. This is possible only if a long series of single-exposed images is acquired so that the number of particles to be taken into account, for the trajectory recognition at each time, does not depend on the total duration of the acquisition. It may be noticed that from a Lagrangian data set, both Lagrangian and Eulerian statistics can be calculated. On the contrary, the calculation of Lagrangian statistics from a Eulerian data set is much more complicated since it involves the integration in time of the instantaneous Eulerian velocity field.

PTV has been applied to a laboratory model of the convective boundary layer of the atmosphere. From trajectory statistics, the probability distribution of transition between different levels has been computed under the assumption of a steady, horizontally homogeneous velocity field in the Eulerian reference frame.

2. Lagrangian statistics

In particle tracking, seeding particles are followed during their motion within the measuring volume, by evaluating the velocity from the displacement of each particle from one image to the next, i.e. the velocity samples are associated with fluid particles rather than merely with a location, i.e. in a Lagrangian reference frame. In general, 3D PTV measurements are possible (Nadeem and Dracos 1993, Virant and Dracos 1996). Nevertheless, in the present experiment only two components of particle location and velocity are determined, this means that only the statistics involving the two measured components are actually evaluable.

Let T be the total acquisition time and Δt the time interval between subsequent images; the position of a particle is known at a discrete series of times $t_j = j\Delta t$, $j = 1, \ldots, N$, where $N = T/\Delta t$. Each successful tracking of a particle gives a trajectory described by the vector (Monin and Yaglom 1971)

$$\boldsymbol{X} = \boldsymbol{X}(m, j) \tag{1}$$

that indicates the position as a function of the particle m and of discrete time j. To identify the particles, a progressive numeration is used instead of the initial position of the particle because not all particles are present at the initial time. Since the particles can leave or enter the measuring volume during the acquisition, the trajectory is known only between its initial time j_{0_m} and its final time j_{f_m}. The

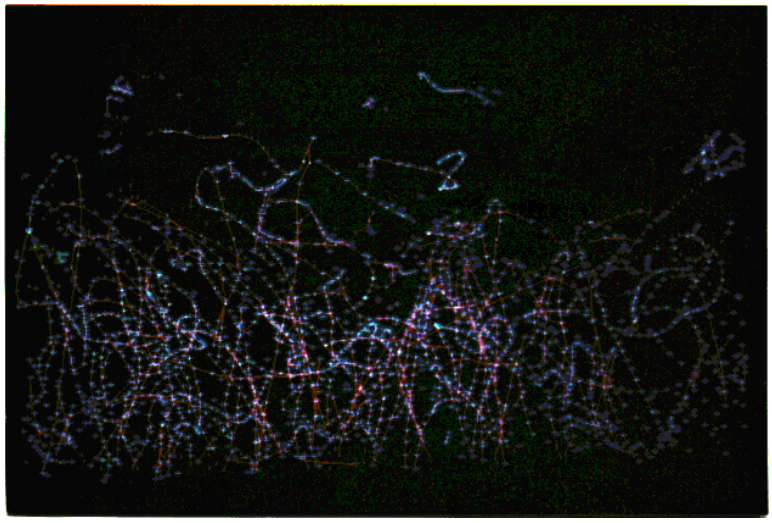

Figure 4. A sequence of superimposed images and trajectories recognized by PTV.
(This figure can be viewed in colour in the electronic version of the article; see http://www.iop.org)

velocity field is expressed as a discrete function of the trajectory (1):

$$\boldsymbol{U}(m,\,j)=\left.\frac{\partial \boldsymbol{X}(m,\,t)}{\partial t}\right|_m=\frac{\boldsymbol{X}(m,\,j+1)-\boldsymbol{X}(m,\,j-1)}{2\Delta t}. \tag{2}$$

In a Eulerian framework, provided that the phenomenon is steady and ergodic, the statistics can be computed from the Lagrangian data by averaging samples of all the trajectories that reach given locations. For example, the mean velocity and the variance on a spatial grid is given, respectively, by:

$$\langle \boldsymbol{u}(\boldsymbol{i})\rangle=\frac{1}{N_{\boldsymbol{i}}}\sum_m\sum_j \boldsymbol{U}|_{\mathbf{G}\cdot\boldsymbol{i}}(m,\,j) \tag{3}$$

and

$$\sigma_k^2(\boldsymbol{i})=\frac{1}{N_{\boldsymbol{i}}}\sum_m\sum_j (U_k|_{\mathbf{G}\cdot\boldsymbol{i}}(m,\,j)-\langle u_{\boldsymbol{i}}(\boldsymbol{i})\rangle)^2 \tag{4}$$

where

$$\mathbf{G}=\begin{pmatrix}\Delta x & 0 & 0\\ 0 & \Delta y & 0\\ 0 & 0 & \Delta z\end{pmatrix}$$

is the spatial discretization tensor,

$$\boldsymbol{i}=\begin{pmatrix}i_x\\ i_y\\ i_z\end{pmatrix}$$

is the vector of the discrete co-ordinate on the grid; the summation is limited to the velocity samples at the location $\mathbf{G}\cdot\boldsymbol{i}$ and $N_{\boldsymbol{i}}$ is the number of samples taken into account.

Furthermore, Lagrangian statistics, such as mean velocity and auto-correlation of a steady (in a Eulerian sense), ergodic, phenomenon are obtained by averaging samples from all the trajectories reaching a given location. The mean velocity is expressed as:

$$\langle \boldsymbol{U}(\boldsymbol{X},n)\rangle=\frac{1}{M_{\boldsymbol{X},n}}\sum_{m|\boldsymbol{X},n}\boldsymbol{U}|_{\boldsymbol{X}}(m,\,j_{\boldsymbol{X},m}+n) \tag{5}$$

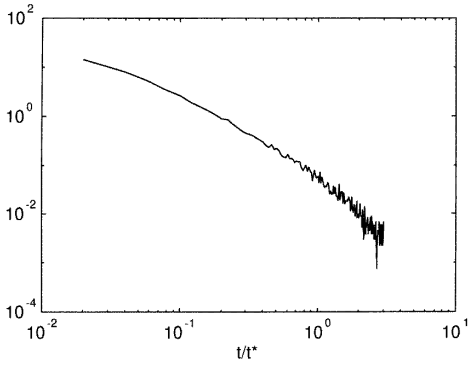

Figure 5. Probability density distribution of trajectory length as a function of the non-dimensional time.

where $j_{\boldsymbol{X},m}$ is the discrete time at which the location is reached and the summation is limited to the $M_{\boldsymbol{X},n}$ trajectories reaching the given location and long enough for the final time to fulfil the condition:

$$j_{f_m}\geq j_{\boldsymbol{X},m}+n. \tag{6}$$

The Eulerian steadiness implies that the summation on the right-hand side of (5) does not depend on the initial time $j_{\boldsymbol{X},m}$, nevertheless the Lagrangian average can be time dependent.

The correlation is:

$$R_{rs}(\boldsymbol{X},n)=\frac{1}{M_{\boldsymbol{X},n}}\sum_{m|\boldsymbol{X}}U_r(m,\,j_{\boldsymbol{X},m})\cdot U_s(m,\,j_{\boldsymbol{X},m}+n). \tag{7}$$

The Lagrangian correlation coefficient is obtained by normalizing $R_{rs}(\boldsymbol{i},n)$ by the velocity variance at location $\boldsymbol{i}$:

$$r_{rs}(\boldsymbol{X},n)=\frac{R_{rs}(\boldsymbol{X},n)}{\sqrt{\langle\sigma_r^2(\boldsymbol{X})\rangle\cdot\langle\sigma_s^2(\boldsymbol{X})\rangle}}. \tag{8}$$

In a Lagrangian framework, the large-scale characteristics of the fluid motion are described by the integral Lagrangian

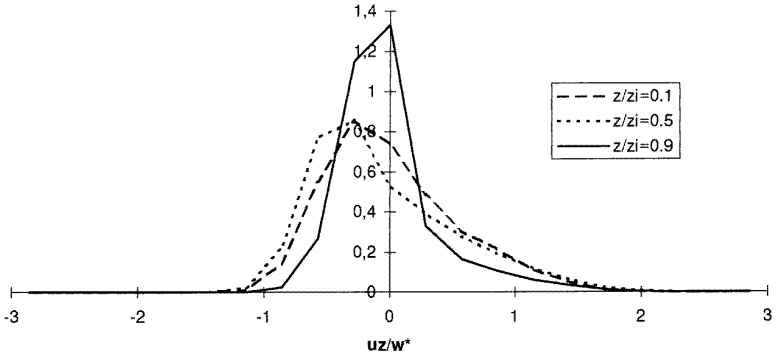

Figure 6. Probability density distribution of the non-dimensional vertical velocity.

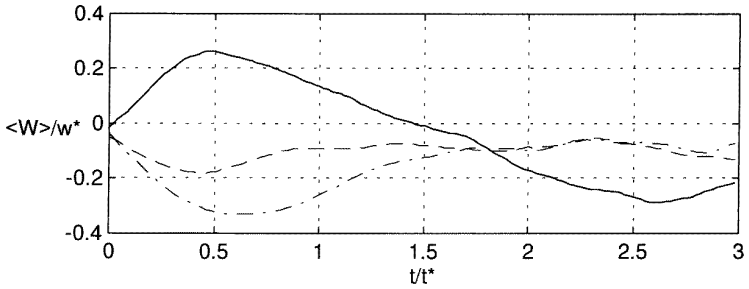

Figure 7. Mean vertical velocity as a function of time in the Lagrangian reference frame at z/z_i = 0.25 (full curve), z/z_i = 0.55 (broken curve), z/z_i = 0.75 (chain curve).

time scale. In a non-homogeneous turbulent flow, such as that indicated in this study, some authors state that the integral of the auto-correlation coefficient is not the Lagrangian integral time scale (Thomson 1987). Nevertheless, the above defined scale plays a fundamental role in Lagrangian stochastic models of particle dispersion also in the case of strong inhomogeneities of the turbulence (Monti and Leuzzi 1996). From a theoretical point of view, it is defined as the integral of the auto-correlation coefficient, and for a discrete time series it is:

$$\tau_{L,r}(\boldsymbol{X}) = \Delta t \cdot \sum_{n=0}^{\infty} r_{rr}(\boldsymbol{X}, n). \tag{9}$$

As a matter of fact, confidence in the evaluation of the auto-correlation coefficient decreases strongly with the time interval n, because the number of relevant trajectories, $M_{\boldsymbol{X},n}$, decreases dramatically. This is why, in order to represent the integral properties of the phenomenon, the 1/e scale, $T_{L,r}$, was chosen. It is defined as the time lag at which the auto-correlation coefficient is reduced to the 1/e value. As a consequence it is computed by taking into account only values of the auto-correlation for small, positive, time lags, where the confidence is still high due to the large number of sufficiently long trajectories.

The transport properties of the phenomenon can be investigated by a statistic that is in between the Lagrangian and Eulerian frameworks: the transilient matrix (Stull 1993). In general, a stochastic process is completely defined by the probability density, $p(\boldsymbol{X}_1, t_1, \boldsymbol{X}_2, t_2)$, of particles starting at time t_1 at location $\boldsymbol{X}_1$, and reaching location $\boldsymbol{X}_2$ at time t_2, that is a function of eight independent variables. The convective boundary layer under investigation can be assumed to be steady and horizontally homogeneous. As a consequence the probability is only function of five independent variables: $p(z_1, z_2, t_2 - t_1, x_2 - x_1, y_2 - y_1)$. Integrating the latter over the horizontal displacements, $\delta x = x_2 - x_1$, $\delta y = y_2 - y_1$, yields the probability that a particle moves from a height z_1 to another height z_2 in a given time interval $\delta t = t_2 - t_1$:

$$\mathrm{tr}(z_1, z_2, \delta t) = \int_{-\infty}^{\infty}\int_{-\infty}^{\infty} p(z_1, z_2, \delta t, \delta x, \delta y)\,\mathrm{d}(\delta x)\,\mathrm{d}(\delta y). \tag{10}$$

This statistic is neither Eulerian, because the starting location of particles is considered, nor Lagrangian because the statistic is not computed along the trajectories. In the case of a discretized height, it is a two-dimensional array function of the time lag δt, whose subscripts indicate the source and destination levels.

3. Experimental set-up

The atmospheric convective boundary layer generated by solar radiation on the soil in the late morning and early afternoon of a sunny day, above a flat terrain, was simulated by a convection chamber filled with water. The mean wind was assumed absent or very light, so that the mechanical production of turbulent kinetic energy is small compared to the buoyant production. In these conditions, the heating

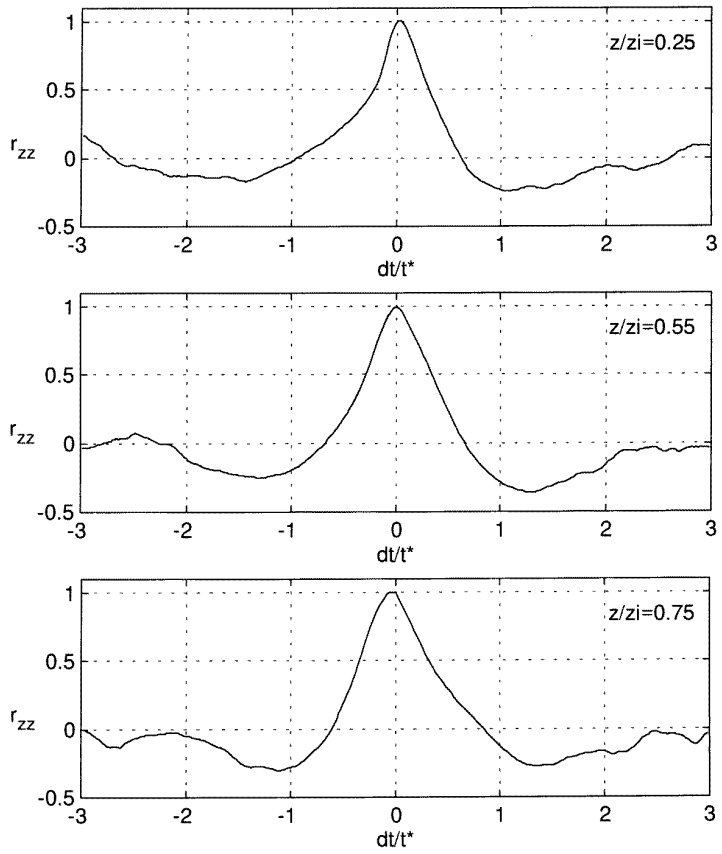

Figure 8. Lagrangian auto-correlation coefficient of the vertical velocity at three different heights.

of the soil generates a convective layer that is bounded from above by a thermally stable layer, namely the capping inversion, that is slowly eroded by entrainment into the lower turbulent layer (figure 1).

A sketch of the convection chamber, whose horizontal dimensions are 41 cm$\times$41 cm is presented in figure 2. From the point of view of the heat we can consider (Cenedese *et al* 1992, Cenedese and Querzoli 1994 and Querzoli 1996):

(i) the bottom, that is an aluminium plate uniformly heated from below, as isothermal;

(ii) the top, insulated by a polystyrene slab to avoid cooling due to evaporation, as adiabatic;

(iii) the side walls, made of glass (0.8 cm thick), as adiabatic.

The following steps are performed during each experiment:

(i) the tank is filled up to 10 cm with ambient temperature water;

(ii) a second layer, 10 cm high, of hot water (20 °C higher than ambient) is stratified above the first one to generate a thermally stable zone that simulates the capping inversion of the atmosphere;

(iii) about 5 min after heat is applied to the lower surface (simulating solar heating of the soil) turbulent convection is completely developed and acquisition starts.

The water is seeded with polystyrene non-buoyant particles whose diameter, 0.2 mm, is trivially much smaller than the scale of the flow under investigation. The number of particles is chosen so that their displacement between two successive analysed images is smaller than the mean distance between the particles. The measuring volume is illuminated by a 1000 W arc lamp placed 2.5 m away from the tank so as to obtain an almost parallel light beam. A beam stop allows the depth of the illuminated area to be controlled. Adjusting the video-camera optics, the particles are acquired in a 10.0 cm high, 12.5 cm wide and 5.0 cm deep volume placed above the lower surface and in the centre of the tank.

The image acquisition and analysis procedure requires the following steps (Querzoli 1996).

(i) Images are acquired by a CCD video-camera and recorded on tape by a video-recorder. During acquisition a frame code is inserted by an animation controller in order to identify each single frame acquired during the subsequent procedure.

(ii) By means of the animation controller one frame in every ten is automatically identified on the tape and digitized by a frame grabber on a 512 $\times$ 512 pixel $\times$ 256 grey level array. The whole procedure is automatically controlled by a personal computer.

(iii) Digitized frames are thresholded and centroids of the particles are computed and stored together with

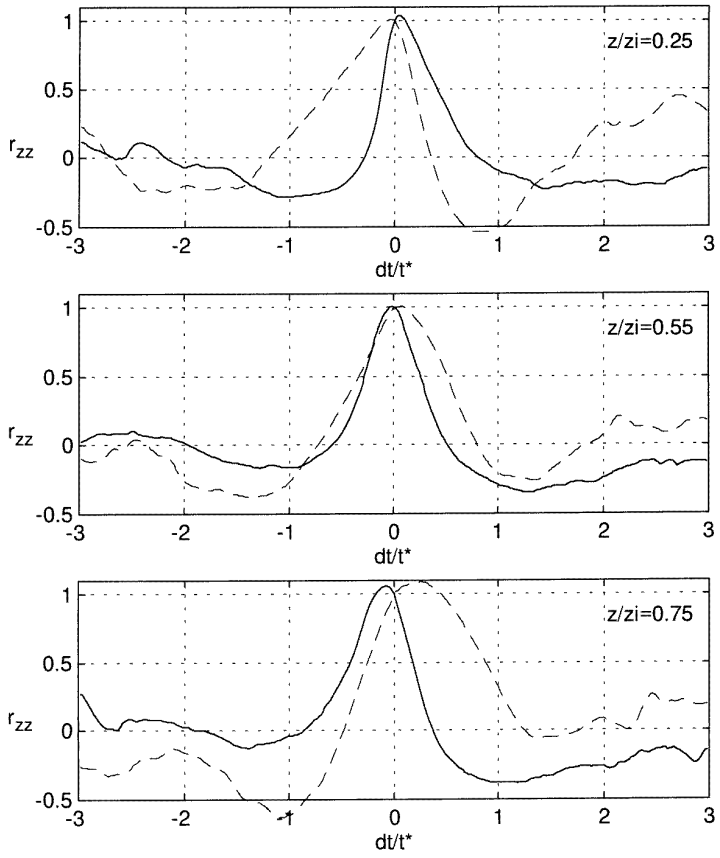

Figure 9. Lagrangian auto-correlation coefficient of the vertical velocity at three heights. Broken curves indicate the downdraughts; full curves updraughts.

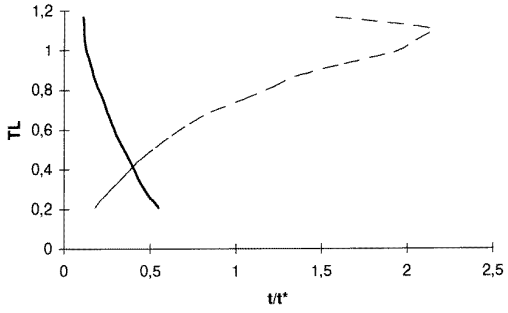

Figure 10. 1/e time scale of the updraughts (full curve) and downdraughts (broken curve) as a function of the non-dimensional height.

time information. Only the resolution of the digitized frame (about 0.2×0.2 mm^2/pixel), not the seeding particle dimensions, affects the accuracy of measuring their positions since the centroids of their images on the frame are considered. This accuracy is of the order of pixel dimensions.

(iv) Trajectories are recognized by looking for time-ordered centroids series that accomplish the following requirements (figure 3):

- the maximum distance between two particle locations must be less than a given value D, i.e. a maximum velocity is assumed for the flow;
- the maximum difference between two successive spots must be smaller than a second, given parameter e, i.e. a maximum acceleration is assumed for the flow;
- a trajectory must consist of at least three particle locations.

The choice of the parameters D and e is crucial: if their values are too small high-speed particles are not tracked. On the other hand, if they are too large, a significant number of errors occurs during the trajectory reconstruction. In figure 4 an example of an acquired and elaborated image is shown.

4. Results

Comparison between atmospheric phenomena and convection occurring in a water tank is possible by using the similarity proposed by Deardorff (1970). It is assumed that the scaling parameters are the convective velocity, $w^* = \sqrt[3]{g\alpha q_s z_i}$, the height of the convective layer z_i and the convective time $t^* = z_i/w^*$, where g indicates the acceleration due to gravity, α the thermal expansion coefficient and q_s the kinematic heat flux at the surface. Results presented

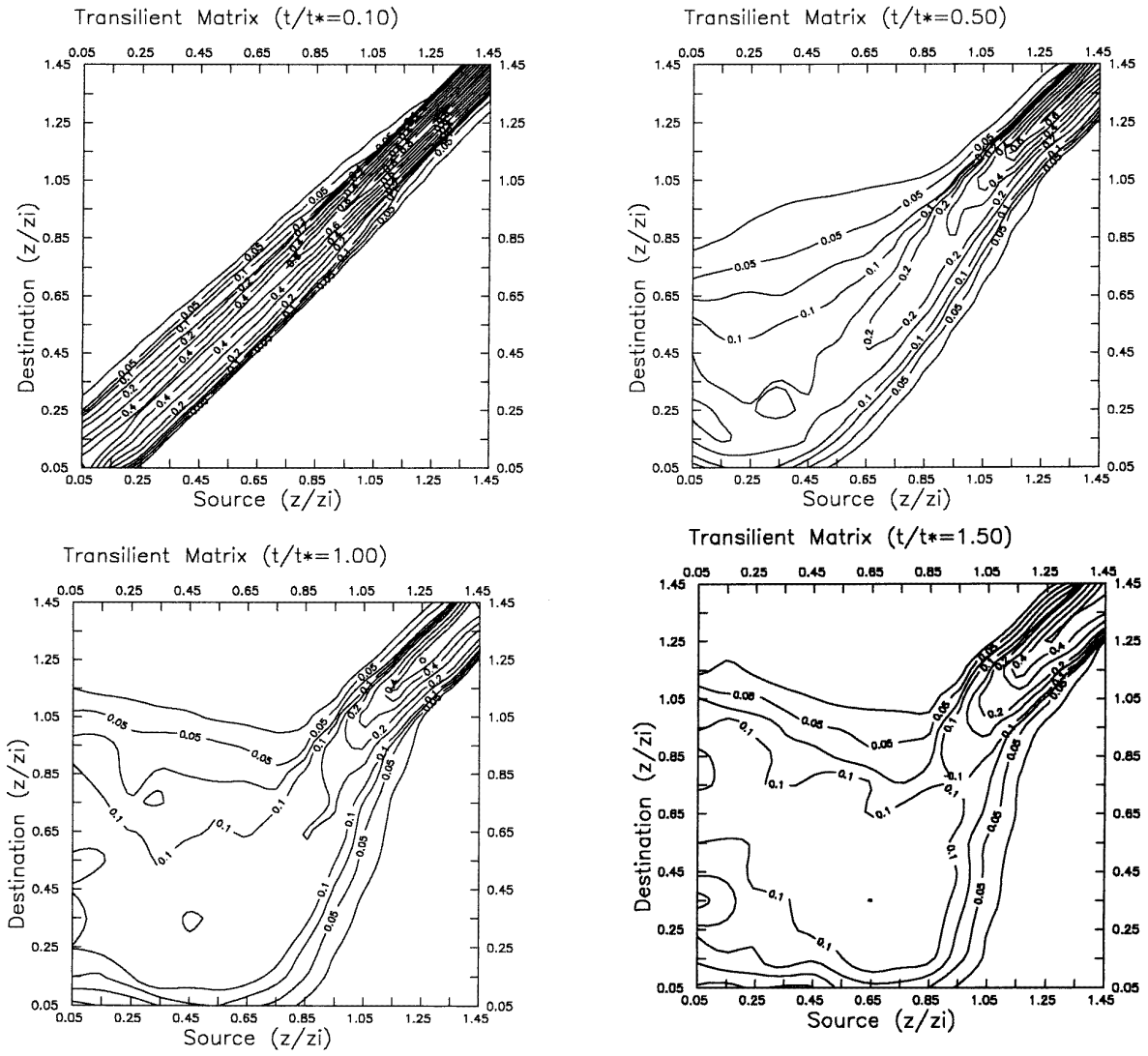

Figure 11. Transilient matrix at different time intervals.

in non-dimensional form throughout this scaling are not dependent on the particular conditions of the experiment. As a consequence, the non-dimensional Eulerian statistics do not vary with time provided that convection is fully developed. It was observed that, 5 min after heating was applied, the vertical profiles of Eulerian non-dimensional statistics obtained from data sampled during different time intervals no longer varied (Cenedese and Querzoli 1994). As a consequence the phenomenon was considered quasi-steady after that time.

Due to the dimensions of the measuring volume and to errors during the tracking, the number of recognized trajectories decreases rapidly with their length. This is shown in figure 5 where the probability density distribution of trajectory length is presented as a function of the non-dimensional time.

In a Eulerian frame of reference, the phenomenon is steady and the probability density distribution of the vertical velocity is not symmetrical, with a slightly negative mode (figure 6). This is due to the fact that the convective boundary layer is characterized by small and intense updraughts and large but slow downdraughts (Willis and Deardorff 1974, Deardorff and Willis 1985, Stull 1988, Hunt *et al* 1988).

The Lagrangian mean vertical velocity, at three different levels, is presented in figure 7, as a function of the non-dimensional time. It is apparent that, although the phenomenon is steady from the Eulerian point of view, this is not true in a Lagrangian framework. The mean velocity varies with time because this statistic is evaluated along the trajectories of particles that move around within the layer, meeting different conditions. Only the asymptotic limit is zero, that is as far as the velocities are completely uncorrelated. The mean velocity of particles starting close to the ground increases for short times because they cross layers with higher velocity, and an opposite trend is observed for the particles starting close to the capping inversion.

The non-symmetry of the Lagrangian auto-correlation coefficient, plotted in figure 8 at three different heights,

confirms the Lagrangian non-steadiness of the phenomenon. Since normalization of the correlation coefficients is done by means of the Eulerian variance at the starting level of the trajectories, they are not defined as less than one as in the case of classical Eulerian coefficients; nevertheless in this way the original shape of the function is preserved.

The different behaviour of the hot updraughts and cold downdraughts has been pointed out by the conditional sampling. The ensemble of trajectories has been divided into two sets: the first one includes trajectories that initially move upwards, the second one trajectories that initially move downwards. Statistics have been computed separately for the two sets (figure 9). The correlation coefficient of the vertical velocity is not maximum for a zero time lag: particles rising from the lower part of the layer ($z/z_i = 0.25$) exhibit a maximum correlation for a slightly positive time lag since they are slow in the proximity of the surface and accelerate through the whole depth of the layer. On the contrary, descending particles found in that region decelerate as they get closer to the lower surface and exhibit the maximum correlation at a negative time lag. This behaviour is not apparent at mid-height ($z/z_i = 0.55$) where no sudden changes in particle velocity are imposed by close boundaries. In the upper part of the layer ($z/z_i = 0.75$) symmetrical behaviour is observed. Due to the presence of the capping inversion ascending particles decelerate and their correlation is a maximum for slightly negative time lags, whereas descending ones accelerate and exhibit the maximum correlation for a positive time lag.

According to this behaviour, the 1/e Lagrangian time scale, T_L, of the vertical velocity, computed for positive time lags (figure 10), increases with height for the updraughts since this scale is related to the time taken by the particles to reach the capping inversion. The behaviour of the descending particles 1/e time scale is different since in this case the scale is related to the time that particles take to reach the lower surface. The downdraught time scales are generally larger than those of the updraughts because the former are characterized by a lower velocity, according to the probability density distribution shown in figure 6.

A more detailed description of the mixing process can be obtained from analysis of the transilient matrix. Assuming horizontal homogeneity, and dividing the investigation field into layers, this matrix represents the fraction of fluid advected from one layer to another in a given time interval. Its first index shows the destination level of mixing and the second the source level. In figure 11 the transilient matrix is presented for four time intervals; the rows of the matrix are plotted in reverse order in order to have the height axis increasing upwards. The elements of the main diagonal indicate the fraction of fluid that does change layer in the given time. For small time intervals mixing is concentrated close to this zone since particles have not had time to mix. As time goes on, larger and larger zones of the matrix are affected by mixing and have non-zero values. For times larger than t^* all the convective layer is mixed ($z/z_i < 1$) whereas the high values of sources and destinations larger than z_i remain concentrated close to the main diagonal, giving evidence that the capping inversion does not participate in mixing phenomena and pollutants are confined in the convective layer.

5. Conclusions

Pollutant dispersion phenomena occurring in the convective boundary layer of the atmosphere have been investigated by means of particle tracking velocimetry. The flow is steady from the Eulerian reference frame but not in the Lagrangian one since particles, during their motion, reach regions that can be considered homogeneous only in the horizontal plane. Vertical homogeneity of Lagrangian statistics is achieved only for very long time intervals, when particles are completely non-correlated to their initial condition. The study has been carried out following the particles only for a few time scales and evidence of vertical homogeneity could not be given.

Since the characteristic timescale of turbulence is of the order of 10 s, a standard video-camera is more than adequate to acquire the successive positions of particles in the measuring volume. As a matter of fact, only one image in every ten was sufficient to separate particle displacements and trajectories. The same technique could be applied to phenomena with shorter characteristic times with a system capable of acquiring and recording images at higher frequencies than those of the investigated flow, for a long enough time (high-speed video-camera).

The evaluation of the transilient matrix permits estimation of the pollutant dispersion whatever the height of the source. Superimposing results from different heights, multiple and distributed sources can be simulated. Finally, assuming that horizontal dispersion is very small compared to transport due to a mean wind, the concentration field downwind from a source in the presence of a mean wind can be simulated by means of the Taylor hypothesis. In fact, the vertical concentration distribution at a distance $\Delta x = \boldsymbol{U}_{wind} \cdot \Delta t$ from the source is obtained by multiplying the transilient matrix at the given Δt by a state vector that is zero everywhere except for the element corresponding to the source height (it represents the vertical concentration distribution at the source location). The procedure can then be iterated downwind using the state vector obtained in the previous step (Stull 1993).

References

Adrian R J 1991 Particle-image techniques for experimental fluid mechanics *Ann. Rev. Fluid Mech.* **23** 261–304

Cenedese A, Franceschi M A and Querzoli G 1992 A laboratory simulation of dispersion phenomena in the atmospheric convective boundary layer *Proc. of Heat and Mass Transfer Forum (Mink, Belorussia)*

Cenedese A and Querzoli G 1994 A laboratory model of turbulent convection in the atmospheric boundary layer *Atmos. Env.* **28** 1901–4

Deardorff J W 1970 Convective velocity and temperature scales for the unstable planetary boundary layer and for Rayleigh convection *J. Atmos Sci.* **27** 1211–13

Deardorff J W and Willis G E 1985 Further results from a laboratory model of the convective planetary boundary layer *Bound.-Layer Meteorol.* **32** 205–36

Hunt C R, Kaimal J C and Gaynor J E 1988 Eddy structure in the convective boundary layer—new measurements and new concepts *Q. J. R. Meteorol. Soc.* **114** 827–70

Keane R D and Adrian R J 1992 Theory of cross-correlation analysis of PIV images *Appl. Sci. Rev.* **19** 191–215

Lorenço L M 1996 *Historical Background, Mathematical tools in PIV, Processing Techniques, von Karman Institute of Fluid Dynamics Lecture Series* (Brussels: VKI)

Monin A S and Yaglom A M 1971 *Statistical Fluid Mechanics* (Cambridge: MIT)

Monti P and Leuzzi G 1996 A clusure to derive a three-dimensional well-mixed trajectory model for non-Gaussian, inhomogeneous turbulence *Bound.-Layer Meteorol.* **80** 311–31

Nadeem A M and Dracos Th 1993 Lagrangian PTV in 3D flows *Appl. Sci. Res.* **51** 161–6

Querzoli G 1996 A Lagrangian study of particle dispersion in the unstable boundary layer *Atmos. Env.* **30** 2821–9

Raffel M and Kompenhans J 1996 *Theoretical and Experimental Aspects of PIV Recording Utilizing Photographic Film and Mechanical Image Shifting, von Karman Institute of Fluid Dynamics Lecture Series* (Brussels: VKI)

Stull R B 1988 *An Introduction to Boundary Layer Meteorology* (Dordrecht: Kluwer)

——1993 Review of transilient turbulence theory and nonlocal mixing *Bound.-Layer Meteorol.* **62** 21–96

Thomson D J 1987 Criteria for selection of stochastic models of particle trajectories in turbulent flows *J. Fluid Mech.* **180** 529–56

Virant M and Dracos Th 1996 An application of 3D-PTV on the measurement of turbulent quantities and particle dispersion in turbulent channel flow *Advances in Turbulence* vol VI, ed S Gavrilakis *et al* (Dordrecht: Kluwer) pp 499–502

Willis G E and Deardorff J W 1974 A laboratory model of the unstable planetary boundary layer *J. Atmos Sci.* **31** 1297–307